Dalton Transactions

Cracking Down on Vapochromic Salts: Unveiling Vapomechanical Stress in Gas-Sorbing Platinum Complexes

Journal:	*Dalton Transactions*
Manuscript ID	DT-ART-07-2024-002053.R3
Article Type:	Paper
Date Submitted by the Author:	04-Nov-2024
Complete List of Authors:	Norton, Amie; Kansas State University, Department of Entomology Taylor, Stephen; University of Cincinnati - East Campus Williams, Caroline; University of Cincinnati - East Campus Zoller, Ann; University of Cincinnati Dietrich, Watts; University of Cincinnati - East Campus Connick, William; University of Cincinnati, Chemistry Chatterjee, Sayandev; TerraPower LLC,

Cracking Down on Vapochromic Salts: Unveiling Vapomechanical Stress in Gas-Sorbing Platinum Complexes

Amie E. Norton,[a,b*1] Stephen D. Taylor, [a,c*1] Caroline Williams,[a] Ann Zoller,[a] Watts Dietrich,[a] William B. Connick,[a, €] and Sayandev Chatterjee[d*]

[a]Department of Chemistry, University of Cincinnati, Cincinnati, OH 45221, United States

[b]Department of Entomology, Kansas State University, Manhattan, KS 66506, United States

[c] The Laboratory Safety Institute, Nantucket, MA 02554, United States

[d]TerraPower LLC, Bellevue, WA 98008, United States

[1] Authors contributed equally

*Corresponding authors' email: amien@ksu.edu; stephen@labsafetyinstitution.org; schatterjee@terrapower.com

ABSTRACT

This study explores the vapochromic and vapoluminescent behaviors of $[Pt(tpy)Cl]PF_6$ host molecules (tpy = 2,2':6',2''-terpyridine) under acetonitrile (CH_3CN) vapor guest, challenging the conventional view that these phenomena arise solely from direct host-guest interactions. Our findings reveal a cooperative mechanism where mechanochromic surface perturbations prime the Pt(II) host for guest incorporation, leading to initial color and luminescence changes prior to significant structural alterations. While the color transition between the yellow $[Pt(tpy)Cl]PF_6$ form and the red/orange $[Pt(tpy)Cl]PF_6$•CH_3CN form is reversible, repeated vapor cycling induces a loss of crystallinity, as indicated by diffraction peak broadening and emission shifts. Scanning electron microscopy analyses show mechanical deformations like bending and surface pitting, emphasizing the role of vapomechanical stress in altering optical properties. These insights highlight the need for integrated design strategies in developing robust vapochromic materials for gas sensing applications.

INTRODUCTION

Advancing technology for monitoring airborne contaminants is crucial for accurate measurements and protecting lives.[1–3] Applications include immediate detection of toxic gaseous chemicals, tracking gaseous plumes, and ensuring air quality in various environments.[4,5] Vapochromic and vapoluminescent materials undergo rapid color or luminescence changes when exposed to specific chemical vapors due to alterations in their electronic structure.[6–10] These changes are often reversible upon removal of the vapor.[10–12]

Notably, small-molecule systems with coordinatively unsaturated square-planar platinum(II) salts are valued for their rich spectroscopic properties, which are heavily dependent on Pt•••Pt distances.[13,14] When paired with ligands that provide access to vacant axial sites, these systems can be finely tuned through non-covalent interactions.[15,16] This tunability has been exploited in various stimuli-responsive systems, where

non-covalent Pt•••Pt interactions are altered by mechanical[17] or thermal stimuli,[9,18,19] confinement within rigid pores,[20] or exposure to molecular vapors solvents,[21–24] or ionic species.[25–29]

Progress in these areas, particularly in vapochromism, has largely stemmed from serendipitous discoveries or modifications of systems found by chance. Understanding vapochromism and vapoluminescence can help develop more effective systems for monitoring and detecting gaseous contaminants. A historical examination of the mechanistic origins of vapochromism in Pt(II) systems has uncovered several assumptions that had resulted in broad generalizations. This study revisits these assumptions through a detailed analysis of the well-established vapochromic salt chloride (2,2':6',2''-terpyridine)platinum(II) hexafluorophosphate, [Pt(tpy)Cl]PF_6 or **1**•PF_6 (shown in **Figure 1**) upon exposure to CH_3CN vapors. The findings highlight the fallacies and oversimplifications in previous interpretations, demonstrating the need for a more nuanced understanding of vapochromism. Additionally, this work seeks to distinguish the core vapochromic responses from other peripheral effects.

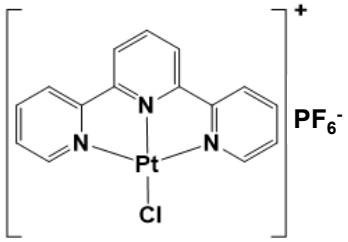

1•PF_6

Figure 1. Molecular structure of the Pt(II) salt investigated in this work: [Pt(tpy)Cl]PF_6 (**1**•PF_6).

Firstly, comprehensive structural characterizations of Pt(II)-vapochromic hosts after exposure to specific guest vapors, as reported in the literature, reveal alterations in Pt•••Pt interactions, primarily due to the incorporation of structurally complementary vapor guests into the Pt(II) host lattice.[30] This has led to the prevalent assumption that both the macroscopic spectroscopic changes—such as striking variations in color and luminescence—and the molecular-level structural modifications are directly triggered by the interaction between the Pt(II) host and the vapor guest.[31,32] However, recent studies, including those from our group and others, indicate that the origin of vapochromism in Pt(II) salts can be more complex.[21–23,33] Our findings presented here, suggest that this process may involve a series of intricate steps. Initial spectroscopic or visible changes upon vapor exposure may result from kinetic effects, where the mechanical interaction of the vapor with the solid perturbs surface Pt(II) molecules without influencing the bulk material. This is supported by alterations in emission spectra without corresponding changes in X-ray diffraction patterns. This study aims to elucidate these mechanisms and assess the role of crystallinity in vapochromic responses.

Secondly, reversibility is a critical aspect of the fundamental understanding and practical application of vapochromic systems. The ability of a system to revert to its original state after exposure to and removal of a vapor influences its recyclability and practical utility. For platinum(II)-based vapochromic systems, reversibility is typically assessed through spectroscopic changes and chemical integrity, the determining factor being the system returning to its original color after one or more cycles of vapor exposure and removal. This study investigates the mechanical effects of CH_3CN vapor absorption and desorption by **1**•PF_6, shedding light on how these effects influence reversibility and providing insight into the mechanisms

of vapochromism. By addressing these aspects, we aim to refine the understanding of vapochromic responses and their implications for practical applications.

METHOD AND MATERIALS

Materials. **1**•PF_6 was prepared according to published procedures.[21,22,27,28] In brief, refluxing Pt(COD)Cl_2 (0.250 grams) and terpyridine (0.180 grams) in DI water (250 mL) for 2.5 hours yielded a red solution of **1**•Cl. The solution was filtered, and NH_4PF_6 was added until yellow powders of unsolvated **1**•PF_6 precipitated. The precipitate was filtered and rinsed three times with 20 mL of water. From the unsolvated **1**•PF_6 powders, yellow needle-shaped crystals were grown by partial evaporation of a 1.5 mM 1:1 acetone/water solution at room temperature. On the other hand, CH_3CN solvated red needles of **1**•PF_6•CH_3CN were grown by partial evaporation of CH_3CN solution at room temperature. Both the solvate and non-solvate crystals were characterized by X-ray Powder Diffraction and X-ray crystallography. The identity and purity of the product was confirmed by ^{1}H NMR spectroscopy, UV-visible spectroscopy, X-ray Powder Diffraction, and mass spectrometry. Analytical data were in agreement with previously published data.[21,22,27,28]

Characterization and Methods. ^{1}H NMR spectra were recorded at room temperature using a Bruker AC 400 MHz NMR. Thin films used in optical spectroscopy measurements were prepared by dissolving the target complex in acetone, followed by rapid evaporation on a hot microscope slide. UV-visible absorption spectra were recorded using a HP8453 diode array spectrometer. Room-temperature steady-state emission spectra were collected using a SPEX Fluorolog-3 fluorimeter equipped with a double emission monochromator and a single excitation monochromator.

Scanning electron microscopy measurements were performed with a FEI XL-30 environmental scanning electron microscope at the Advanced Characteristic Center, University of Cincinnati, Ohio. Samples were imaged without conductive coatings, using secondary electron detection at a 15 kV accelerating potential and a 5.6 μm spot size.

Optical videos of crystals during vapor exposure and desorption were created from still images captured with a Keyence Digital Microscope VHX-1000 at 1000X magnification. Images were taken every 15 seconds over a 15-hour period, covering a full vapor absorption/desorption cycle. Videos were assembled using Windows Live Movie Maker.

X-ray powder diffraction data for freshly prepared samples were collected at the Advanced Photon Source station 11-BM at Argonne National Laboratory, using 0.458884 Å photons, as previously described.[22,28] For vapor cycling experiments, diffraction data were recorded using a Panalytical X-ray powder diffraction instrument with a Cu Kα (λ = 1.54 Å) source. Desolvated specimens were exposed to CH_3CN vapor in a sealed ~1 L glass chamber at room temperature for 24 hours, unless otherwise noted. For cycling experiments, unsolvated **1**•PF_6 crystals were sprinkled onto a microscope slide and immobilized with a thin layer of grease. After five cycles of vapor absorption/desorption (see Fig. SI 2), non-adhering crystals were removed by gently shaking the slide. The slide was placed in the fluorimeter chamber, where CH_3CN vapor was introduced via argon flow. Solvate was removed by flowing argon into the chamber for 20-32 hours at room temperature, followed by flowing argon heated to 140^{0}C for 5 minutes.

RESULTS AND DISCUSSION

Vapochromic Response of **1**•PF_6.

The vapochromic response of **1**•PF_6 is consistent with previous reports.[16,24,34] When exposed to acetonitrile at room temperature, **1**•PF_6 changes from yellow to red/orange (**Fig. 2**). For simplicity, we refer to the observed color as "red". As suggested by the color changes in the species generated via CH_3CN vapour sorption/desorption cycles in **Figure 2**, the response seems reversible. Both yellow and red forms produced during each cycle are visually indistinguishable. ^1H NMR and gravimetric analyses confirmed the uptake of approximately one equivalent of acetonitrile by **1**•PF_6 crystals. This behaviour is consistent with previous reports on the vapochromic response of **1**•PF_6 to CH_3CN vapours. The diffraction pattern of the yellow form closely aligns with the previously reported structure of **1**•PF_6•CH_3CN while that of the red/orange form corresponds to the structure of **1**•PF_6•CH_3CN.

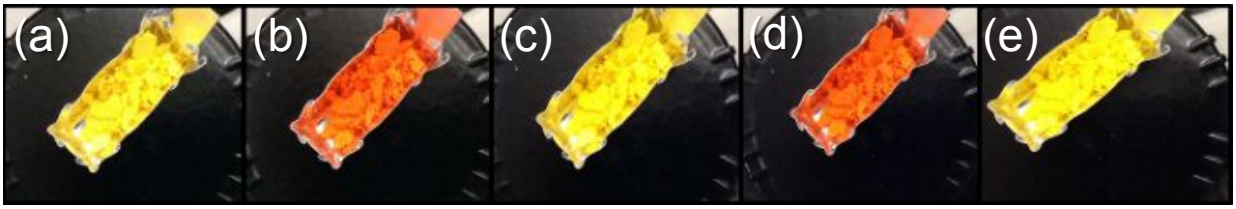

Figure 2. Photographs of a ground sample of yellow **1**•PF_6 in an aluminum weigh boat (a) pre-CH_3CN exposure and (b-d) for two CH_3CN sorption and desorption cycles. (b) Post CH_3CN sorption in the first cycle, (c) post CH_3CN desorption in the first cycle, (d) post CH_3CN sorption in the second cycle, (c) post CH_3CN desorption in the second cycle.

The diffraction pattern of the yellow form closely aligns with the previously reported structure of **1**•PF_6, while that of the red/orange form corresponds to the structure of **1**•PF_6•CH_3CN. Examining the structure of **1**•PF_6 as reported by Taylor et al.,[28] the $Pt(tpy)Cl^+$ cations are arranged in head-to-tail dimers, characterized by alternating short intradimer and longer interdimer Pt•••Pt distances of 3.35 Å and 4.03 Å, respectively. In contrast, the structure of **1**•PF_6•CH_3CN reveals a head-to-tail stacking of $Pt(tpy)Cl^+$ units with a uniform Pt•••Pt separation of 3.37 Å, leading to the formation of an extended, quasi-one-dimensional chain.[21,34] The exposure to CH_3CN results in a cumulative shortening of the Pt•••Pt distances, thereby enhancing the Pt•••Pt interactions. A detailed comparison between the two structures indicates that this shortening in the red/orange form is driven by the incorporation of CH_3CN molecules into the crystal lattice. These observations are consistent with the vapochromic response described by Cao *et al*.[34] Furthermore, when yellow **1**•PF_6 powder or crystals were exposed to CH_3CN vapor for 24 hours, the resulting diffraction pattern closely matched the structure of **1**•PF_6•CH_3CN (Figure SI 3-4). Conversely, heating **1**•PF_6•CH_3CN at 150°C restored the diffraction peaks corresponding to **1**•PF_6 without the formation of intermediates. Thus, vapor absorption and desorption appear to result in a straightforward **A→B** conversion of the solvated crystal form to the desolvated one, without the formation of intermediates. This sorption-desorption process could be repeated multiple times without any discernible differences in the color changes of the final products.

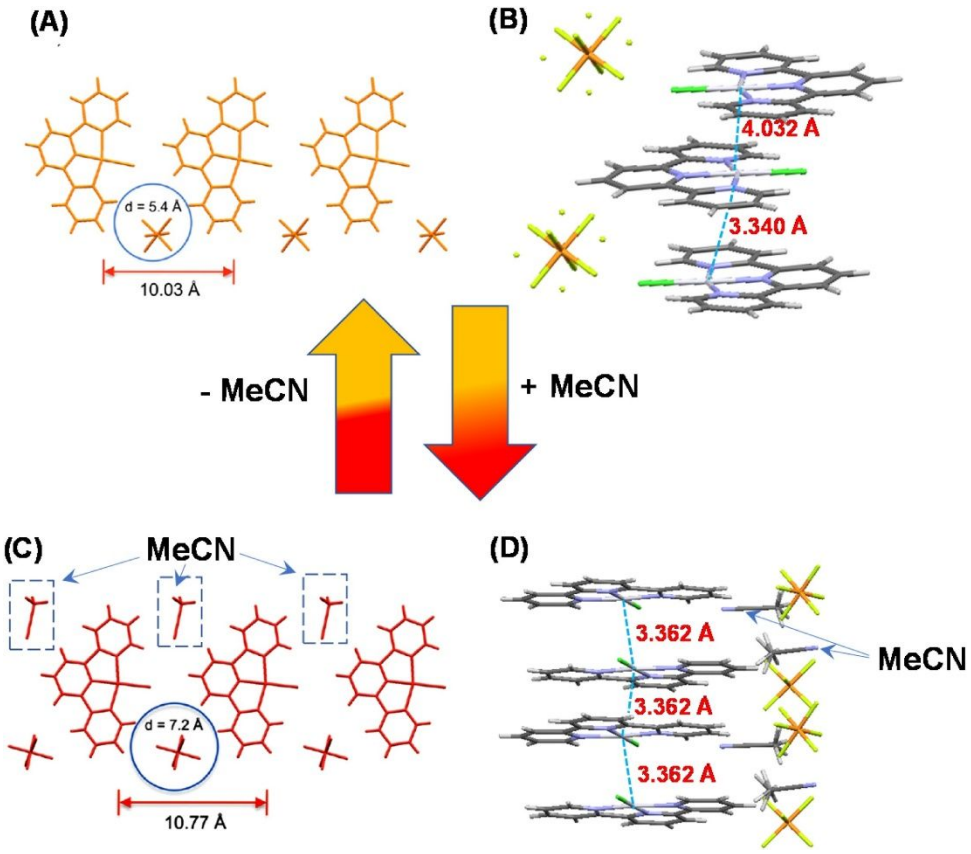

Figure 3 Crystal structures of **1**•PF_6 (A and B) and **1**•PF_6•CH_3CN (C and D). (Adapted with permission from Zhang et al.[34] Copyright (2020) Royal Society of Chemistry).

VAPOR-CYCLING EFFECTS

X-Ray Powder Diffraction. The X-ray Powder Diffraction spectrum of **1**•PF_6 microcrystals (100 mg) were recorded before exposure to CH_3CN, after 24 hours of exposure, and following desorption under ambient conditions. This cycle was repeated three additional times to assess the reversibility of the vapochromic response. Consistent emission maxima in the luminescence spectra (discussed in the following section) and the X-ray diffractograms confirmed the reversible nature of the transformation between the yellow **1**•PF_6 and red/orange **1**•PF_6•CH_3CN forms across cycles. However, a detailed analysis of the diffractograms revealed subtle but significant changes. Specifically, the resolution and intensity of diffraction peaks progressively decreased over the three cycles of CH_3CN vapor absorption and desorption. Representative X-ray Powder Diffraction patterns from these cycles are presented in **Figure S5**.

In the desolvated yellow **1**•PF_6 form, the peak intensity at a 2θ value of 9.5°, decreased by 58% after the first full CH_3CN vapor absorption/desorption cycle (**Figure 3a**). The red/orange form exhibited a 29% reduction in the peak intensity at 2θ of 8.85°, following the first cycle. The reduction rate was less pronounced while the intensity decreased in subsequent cycles. The yellow and red/orange forms showed broader peaks with increasing full width at half maximum (FWHM), and the FWHM increments diminished with each cycle (**Figure 4b**). The crystal sizes and strains are shown in **Figures 4c-d**. The decrease in peak intensity and broadening of the diffraction peaks align with a progressive loss of long-range order in the

crystal structure with each absorption/desorption cycle. Notably, the most significant disruption to the crystalline order occurs during the first cycle of vapor absorption and desorption.

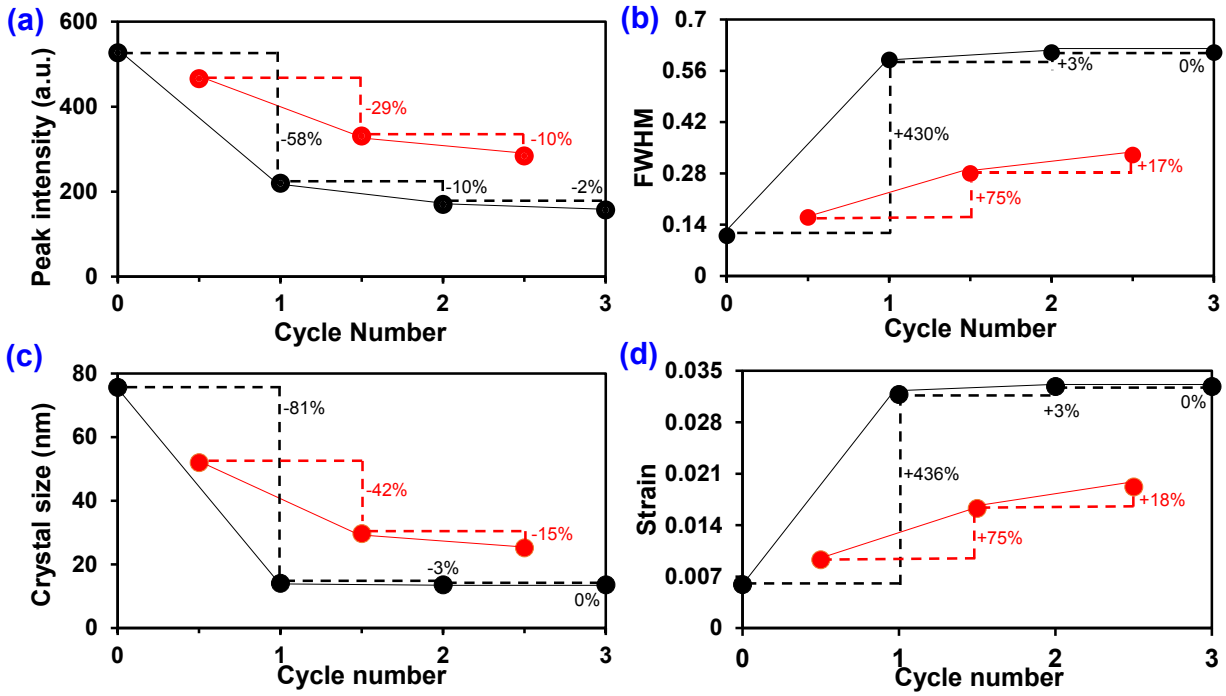

Figure 4. (a) The variation of the representative XRD peak intensities as a function of the CH_3CN vapor absorption/desorption cycle number: At a 2θ of 9.5° the non-solvated yellow form **1**•PF_6 (●, (black)) and at 8.85° for the solvated form **1**•PF_6•CH_3CN (●, (red)). (b) The FWHM of the respective peaks in the diffractograms of the non-solvated form and the solvated form as a function of cycle number. (c) Crystal size of the respective peaks in the diffractograms calculated using the formula ($\tau=\frac{K\lambda}{\beta cos\theta}$) . (d) Strain of the respective peaks in the diffractograms of the non-solvated form calculated using the formula ($\frac{\beta}{4tan\theta}$) .

Luminescence Spectroscopy.

The reversibility of the material's response to CH_3CN exposure was further evaluated using emission spectroscopy (λ_{ex} = 436 nm). The crystals of **1**•PF_6 exhibit green luminescence, characterized by an asymmetric emission band with a maximum at 552 nm (FWHM = 3483 cm^{-1}). This emission maximum is notably shifted from the 630 nm maximum reported at room temperature by Bailey and colleagues, instead aligning more closely with the emission maximum of 565 nm they observed at 77K.[14] Previous studies have demonstrated that the emission spectra of square-planar Pt(II) complexes are highly sensitive to sample preparation and history[35], as noted by Miskowski and Holding, who observed batch-dependent variations in emission maxima for $[Pt(bpy)_2](ClO_4)_2$ and different batches of solid [Pt(1,10-phenanthroline)$_2$](Cl_2).[49] These discrepancies have been attributed to the presence of multiple emissive sites, possible polymorphism, or varying hydration states. Despite their significance, the origins and implications of these effects in the context of vapochromism remain largely unexplored.

Upon exposure to CH_3CN vapor for 48 hours, the material exhibits red emission peaking at 693 nm with an FWHM of 3774 cm^{-1} and a shoulder near 600 nm. An additional 2-hour exposure to acetonitrile did not

show any changes in the emission spectrum. The samples were desorbed under Argon for 24 hours and had not changed, so the sample was heated for 5 minutes to 100°C while simultaneously exposing it to an Argon flow. The heating was then stopped, and Argon then flowed for 1 more hour; if the emission spectra had not changed, heating was applied to the outside of the glass bubbler at 100°C for an additional 5 minutes. This was done until the sample remained unchanged after 2 heating cycles. The yellow species exhibits an emission maximum at 602 nm with FWHM of 3855 cm^{-1} (Fig. 5a, Fig. SI 6-12). The yellow species yielded here also had an X-ray powder diffraction that matches that of pristine **1**•PF_6.

This CH_3CN absorption/desorption process was repeated four more times as shown in **Figure 5a**, and with each cycle, slight variations were observed in the emission features of both the CH_3CN-exposed and CH_3CN-removed states. For instance, although the emission maximum for the yellow form remained relatively stable at 602 nm, the blue edge of the emission band lost intensity. In contrast, the red edge gained intensity with each cycle. A similar trend was noted in the red forms, where the emission maximum remained around 700 nm, but the shoulder at 602 nm gradually diminished, and a slight increase in intensity was observed at the red edge. Throughout these cycles, a progressive decrease in overall emission intensity was noted (**Figure SI 6-12**). The time required to absorb acetonitrile vapor completely decreased with each cycle, going from 48 hours for the first cycle to 18 hours for the last cycle (**Figure 5b**). Thus, the rate at which the material absorbed acetonitrile appeared to increase with vapor cycling. It was impossible to assess changes in the desorption rate because heating the air to complete this step was necessary (**Figure SI 7**). The sorption and desorption processes might induce physical stresses and morphological changes on the surface, potentially increasing the surface area and accelerating the response. Repeated cycling could also create more CH_3CN traps, reducing the 550 nm contribution to the blue edge of the emission band. The most significant effect of cycling was the reduction in time needed to complete the absorption steps, as determined by the point at which the emission spectrum stabilized. While these observations hint at a possible vapomechanical behavior, further investigation is needed to confirm the role of physical stresses and surface morphological changes in enhancing vapochromic responses.

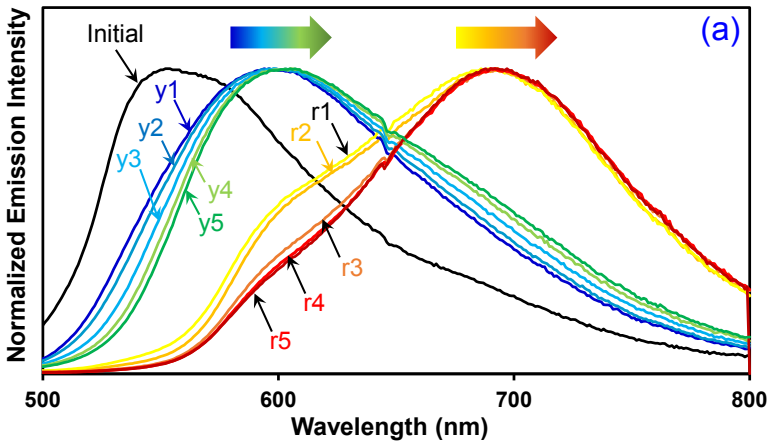

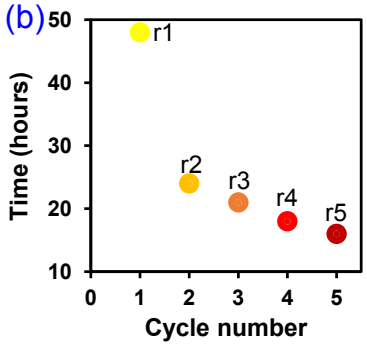

Figure 5. (a) Normalized emission spectra of crystals of **1**•PF_6 before (——) and during CH_3CN uptake and removal: (——, (yellow) r1) first CH_3CN sorption, (——, (blue) y1) first CH_3CN removal, (——, (yellow) r2) second CH_3CN sorption, (——, (blue) y2) second CH_3CN removal, (——, (orange) r3) third CH_3CN sorption, (——, (aqua) y3) third CH_3CN removal, (——, (red) r4) fourth CH_3CN sorption, (——, (bright green) y4) fourth CH_3CN removal, (——,(maroon) r5) fifth CH_3CN sorption, (——, (Kelly green) y5) fifth CH_3CN removal. (b) Time taken to form fully sorbed species as a function of the cycle number.

Probing Vapomechanical Effects via Microscopy

The mechanical effects of vapor absorption and desorption observed in **1**•PF_6 crystals provide further insight into the changes in luminescence behavior discussed earlier. When exposed to acetonitrile vapor, these crystals undergo a shift in emission properties and exhibit pronounced physical alterations such as striations, bending, splitting, and fracturing. In one experiment, a collection of seventeen yellow needle-like crystals, lightly coated with paratone oil to slow vapor uptake, was photographed under a microscope while exposed to acetonitrile vapor (**Figure SI 13**). Over 15 hours, the crystals transitioned to red, with the first signs of this color change appearing within 45 minutes. The average onset of the color change was around 2.5 hours, with the full transition completing in approximately 5 hours. A time-lapse video constructed from these images shows that 10 of the 16 crystals experienced bending, shifting, splitting, or rotation during vapor(**ESI**), underscoring the significant mechanical stresses induced by the vapor interaction. The initial and final images are shown in Figure SI 13.

This mechanical response correlates with the changes observed in the luminescence spectra, where a shift and broadening of emission peaks were noted after the first absorption/desorption cycle. The physical movements and deformations of the crystals, particularly the bending and rotation observed just before or after the complete color change, suggest that these stresses disrupt the emissive states of the material, contributing to the altered luminescence. Notably, the color change typically began at the edges of the crystals and propagated toward the center, aligning with the observation that the blue edge of the emission band loses intensity while the red edge gains intensity with each cycle.

To further understand the impact of these mechanical effects on crystal quality, SEM images were recorded before and after acetonitrile exposure (**Figure 6**). These structural changes mirror the progressive loss of emission intensity observed with repeated cycles, where the vapor-induced mechanical stresses likely alter the crystallinity and surface morphology, thus affecting the luminescent properties. Additional damage was evident after subsequent cycles, with increasing surface pits suggesting that the vapor diffusion pathways

changed after the initial cycles. Initially, the color changes in **1**•PF_6•CH_3CN crystals originated along the long edges, but by the second cycle, the color change was more uniformly distributed across the crystal, indicating a shift in the mechanical response.

These findings suggest that the mechanical stresses induced by vapor absorption and desorption contribute to the observed changes in crystallinity and play a presumptive role in modulating the vapochromic and luminescent responses. The inability to maintain single-crystal X-ray diffraction quality during these processes further underscores the complexity of the vapomechanical effects, which likely enhance the overall changes in both color and emission.

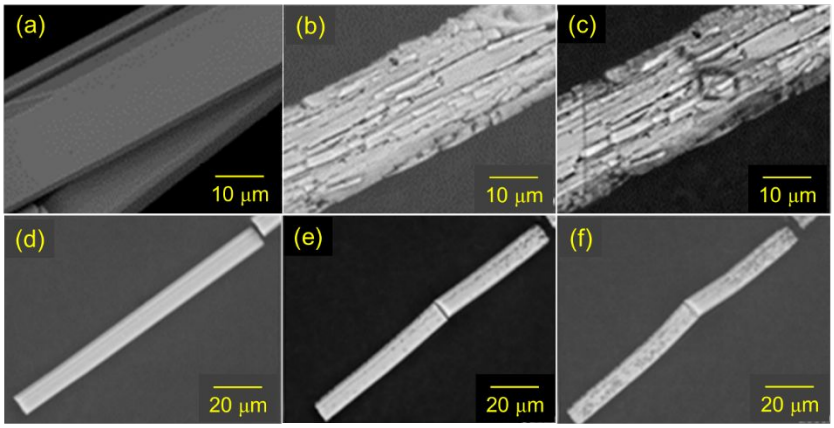

Figure 6. Representative scanning electron micrographs: Crystals of **1**•PF_6 (a) before exposure to acetonitrile, (b) after acetonitrile vapor absorption/desorption, and (c) after a second absorption/desorption cycle. Crystals of **1**•PF_6•CH_3CN (d) before desorption (e) after one cycle of absorption/desorption (f) after a second absorption/ desorption cycle

Impact of mechanical effects on luminescence

We studied how introducing defects through mechanical means affects the luminescence behavior of 1•PF_6 crystals, hypothesizing that it would cause a red shift in the emission spectrum. We subjected a single batch of 1•PF6 crystals to grinding with a mortar and pestle to test this hypothesis. Initially, the crystals exhibited an asymmetric emission band centered at 552 nm (FWHM = 3120 cm^{-1}) with a shoulder at 580 nm (λ_{ex} = 436 nm). Grinding the crystals into a fine powder caused the emission band to broaden and introduced a new shoulder at longer wavelengths, as shown in **Figure 7a**. Subsequent grinding cycles further broadened the emission band and intensified the long-wavelength shoulder, eventually becoming pronounced enough to resemble a peak at 635 nm after six cycles.

These observations underscore mechanical force's significant role in modulating the red shift's extent. The degree of emission shift correlates with the intensity and duration of the grinding process and physical parameters such as the sample's history and pedigree. Variations in these factors influence defect formation and the observed redshift. Additionally, ball mill trials demonstrated even more pronounced effects: the emission band broadened from a FWHM of 3120 cm^{-1} to 3790 cm^{-1}, and the emission maximum shifted from 552 nm to 670 nm (**Figure 7b**). These results confirm that mechanical forces enhance Pt(II)-Pt(II) interactions and affect emission properties, although the shift is less pronounced compared to exposure to CH_3CN (as shown in Figure 7c for comparison). The variability in redshift highlights the influence of

mechanical processing conditions and intrinsic sample properties, supporting our hypothesis that mechanical effects significantly impact the vapochromic and vapoluminescent behavior of the crystals and revealing the underlying complexities of vapochromism.

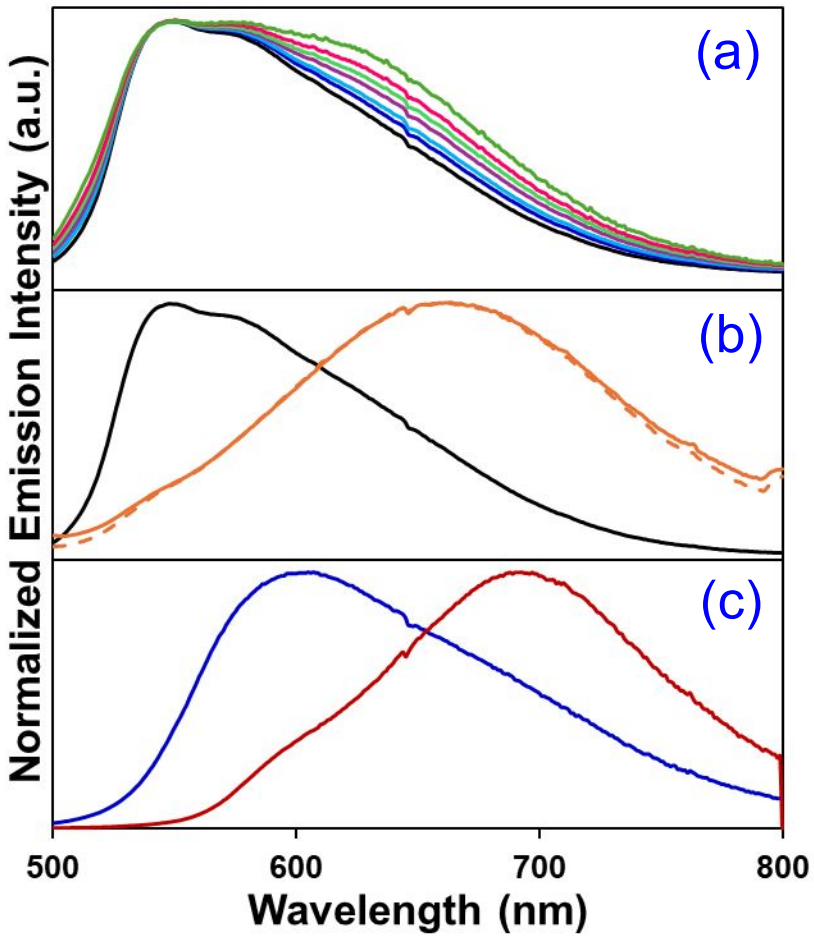

Figure 7. (a) Normalized emission spectra of crystals of **1**•PF_6 before (——) and after grinding with mortar and pestle: (——, (blue)) after first grinding, (——, **(aqua)**) after second grinding, (——, (purple)) after third grinding, (——, (green)) after fourth grinding, (——, (red)) after fifth grinding, (——, (Kelly green)) after sixth grinding. (b) Normalized emission spectra of crystals of **1**•PF_6 before (——) and after ball milling: (solid orange line) after ball milling at room temperature, (dashed orange line (samples grown on the oven at 60 °C and ball milling) (c) **1**•PF_6 before (——, (blue)) and after exposure to CH_3CN (——, (red))

Impact of Mechanical Effects on X-ray Powder Diffraction

To investigate whether mechanical perturbations induce structural defects in **1**•PF_6 crystals, we systematically examined the impact of mechanical stress on their crystal structure. Yellow needle-shaped crystals of unsolvated **1**•PF_6, grown from an acetone/water solution at room temperature, were selected as the most pristine form, free from mechanical distortions. X-ray Powder Diffraction patterns of these pristine crystals were compared to those obtained after extensive mechanical grinding of the crystals into powder. As illustrated in **Figure 8**, the diffractograms of the pristine and ground samples reveal no significant differences, indicating that the crystal structure remains intact post-grinding. These findings

suggest that mechanical perturbations do not alter the short-range order of the crystal lattice, implying that any mechanical effects are likely confined to disrupting long-range interactions and order.

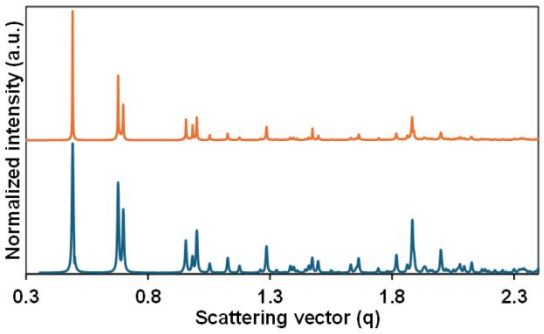

Figure 8. X-ray Powder Diffraction of **1**•PF_6 crystals grown from an acetone/water solution at room temperature: (blue trace) pre-grinding, (orange trace) post-grinding.

CONCLUSIONS

This study offers a nuanced perspective on the vapochromic and vapoluminescent behaviors of **1**•PF_6 in response to CH_3CN vapor. Using this system as a test case, our findings challenge the prevailing assumption that vapochromism originates solely from direct host-guest interactions at the molecular level. Instead, the evidence suggests a multifaceted mechanism where initial colorimetric and luminescent changes are driven by surface perturbations, which precede more significant structural alterations manifesting with prolonged vapor exposure.

These observations suggest a cooperative mechanism in which the phenomenon of vapochromism is not solely initiated by the incorporation of a guest molecule. Initial perturbations occur at the Pt(II) host surface through mechanochromism, priming the host molecule by orienting it in a manner conducive to guest incorporation. This is evidenced by color or spectroscopic changes that occur prior to exposure to CH_3CN vapors, without corresponding alterations in the X-ray diffractogram. Following this preparatory phase, subsequent exposure to the vapors induces more pronounced structural changes in the bulk material, as reflected in the significant shifts observed in X-ray diffraction patterns.

The reversible nature of the color transition between yellow **1**•PF_6 and red/orange **1**•PF_6•CH_3CN forms was confirmed through spectroscopic and diffraction techniques. However, the observed progressive loss of crystallinity with repeated vapor absorption and desorption cycles indicates that this reversibility has limitations. The reduction in diffraction peak intensity and broadening, along with shifts in emission maxima, suggest a gradual disruption of long-range order and emissive states influenced by both chemical and mechanical stresses.

Microscopic and SEM analyses further reveal the extent of mechanical deformation—bending, splitting, and surface pitting—during vapor exposure, underscoring the critical role of vapomechanical effects in modulating the observed optical responses. These mechanical stresses,

likely induced by vapor absorption, appear to affect both crystallinity and luminescent properties over successive cycles significantly.

In conclusion, this study deepens our understanding of the intricate processes governing vapochromism and vapoluminescence in Pt(II) complexes and highlights the importance of considering mechanical effects when designing future materials for gas sensing and other applications. The findings advocate for a more integrated approach to developing vapochromic systems, where both chemical interactions and physical forces are meticulously engineered to optimize performance and durability.

ACKNOWLEDGEMENTS

The Authors thank Drs. Christian Reber and Harry Gray, for reviewing this and helpful suggestions. The ALS is supported by the Director, Office of Science, Office of Basic Energy Sciences, of the U.S. Department of Energy under Contract No. DE-AC02-05CH11231. The authors would like to thank Mrs. Crystal Ly for the graphic image. X-ray Powder Diffraction data was collected at the Advance Photon Source (APS) Beamline 11-BM. We thank Dr. Melodie Finkenscher and Necati Kaval for their expert technical assistance and helpful discussions. This publication was developed under STAR Fellowship Assistance Agreement FP-91765901, awarded by the U.S. Environmental Protection Agency (EPA). The EPA has not formally reviewed it. The views expressed in this publication are solely those of the publisher, and EPA does not endorse any products or commercial services mentioned. This work is dedicated to the memory of Prof. William B Connick who passed away on April 22, 2018.

References

(1) Baum, J. S.; Norton, A. E. In Your Face: Consideration of Higher Risks for Chemical Exposure to Persons with Disabilities in Laboratories. *Journal of Chemical Health & Safety* **2019**, *26* (6), 45–64.
(2) Norton, A. E.; Doepke, A.; Nourian, F.; Connick, W. B.; Brown, K. K. Assessing Flammable Storage Cabinets as Sources of VOC Exposure in Laboratories Using Real-Time Direct Reading Wireless Detectors. *Journal of chemical health & safety* **2018**, *25* (5), 2–9.
(3) Hanna, S. R.; Chang, J.; Strimaitis, D. Hazardous Gas Model Evaluation with Field Observations. *Atmospheric Environment. Part A. General Topics* **1993**, *27* (15), 2265–2285.
(4) Bruno, P.; Caselli, M.; De Gennaro, G.; Iacobellis, S.; Tutino, M. Monitoring of Volatile Organic Compounds in Non-Residential Indoor Environments. *Indoor Air* **2008**, *18* (3).
(5) Halios, C. H.; Landeg-Cox, C.; Lowther, S. D.; Middleton, A.; Marczylo, T.; Dimitroulopoulou, S. Chemicals in European Residences–Part I: A Review of Emissions, Concentrations and Health Effects of Volatile Organic Compounds (VOCs). *Science of the Total Environment* **2022**, *839*, 156201.
(6) Kobayashi, A.; Dosen, M.; Chang, M.; Nakajima, K.; Noro, S.; Kato, M. Synthesis of Metal− Hydrazone Complexes and Vapochromic Behavior of Their Hydrogen-Bonded

Proton-Transfer Assemblies. *Journal of the American Chemical Society* **2010**, *132* (43), 15286–15298.
(7) Takahashi, E.; Takaya, H.; Naota, T. Dynamic Vapochromic Behaviors of Organic Crystals Based on the Open–Close Motions of S-shaped Donor–Acceptor Folding Units. *Chemistry–A European Journal* **2010**, *16* (16), 4793–4802.
(8) Minei, P.; Pucci, A. Fluorescent Vapochromism in Synthetic Polymers. *Polymer International* **2016**, *65* (6), 609–620.
(9) Drew, S. M.; Janzen, D. E.; Buss, C. E.; MacEwan, D. I.; Dublin, K. M.; Mann, K. R. An Electronic Nose Transducer Array of Vapoluminescent Platinum (II) Double Salts. *Journal of the American Chemical Society* **2001**, *123* (34), 8414–8415.
(10) Grove, L. J.; Rennekamp, J. M.; Jude, H.; Connick, W. B. A New Class of Platinum (II) Vapochromic Salts. *Journal of the American Chemical Society* **2004**, *126* (6), 1594–1595.
(11) Daws, C. A.; Exstrom, C. L.; Sowa, J. R.; Mann, K. R. "Vapochromic" Compounds as Environmental Sensors. 2. Synthesis and near-Infrared and Infrared Spectroscopy Studies of [Pt (Arylisocyanide) 4][Pt (CN) 4] upon Exposure to Volatile Organic Compound Vapors. *Chemistry of materials* **1997**, *9* (1), 363–368.
(12) Minei, P.; Koenig, M.; Battisti, A.; Ahmad, M.; Barone, V.; Torres, T.; Guldi, D. M.; Brancato, G.; Bottari, G.; Pucci, A. Reversible Vapochromic Response of Polymer Films Doped with a Highly Emissive Molecular Rotor. *Journal of Materials Chemistry C* **2014**, *2* (43), 9224–9232.
(13) Yip, H.-K.; Cheng, L.-K.; Cheung, K.-K.; Che, C.-M. Luminescent Platinum (II) Complexes. Electronic Spectroscopy of Platinum (II) Complexes of 2, 2′: 6′, 2 ″-Terpyridine (Terpy) and p-Substituted Phenylterpyridines and Crystal Structure of [Pt (Terpy) CI][CF 3 SO 3]. *Journal of the Chemical Society, Dalton Transactions* **1993**, No. 19, 2933–2938.
(14) Bailey, J. A.; Hill, M. G.; Marsh, R. E.; Miskowski, V. M.; Schaefer, W. P.; Gray, H. B. Electronic Spectroscopy of Chloro (Terpyridine) Platinum (II). *Inorganic Chemistry* **1995**, *34* (18), 4591–4599.
(15) Chatterjee, S.; Fujimoto, M. S.; Du, Y.; Hall, G. B.; Lahiri, N.; Walter, E. D.; Kovarik, L. Redox-Based Electrochemical Affinity Sensor for Detection of Aqueous Pertechnetate Anion. *ACS Sens.* **2020**, *5* (3), 674–685. https://doi.org/10.1021/acssensors.9b01531.
(16) Muro, M. L.; Daws, C. A.; Castellano, F. N. Microarray Pattern Recognition Based on PtII Terpyridyl Chloride Complexes: Vapochromic and Vapoluminescent Response. *Chemical communications* **2008**, No. 46, 6134–6136.
(17) Norton, A. E.; Abdolmaleki, M. K.; Liang, J.; Sharma, M.; Golsby, R.; Zoller, A.; Krause, J. A.; Connick, W. B.; Chatterjee, S. Phase Transformation Induced Mechanochromism in a Platinum Salt: A Tale of Two Polymorphs. *Chemical Communications* **2020**, *56* (70), 10175–10178.
(18) Rachford, A. A.; Castellano, F. N. Thermochromic Absorption and Photoluminescence in [Pt (Ppy)(μ-Ph2pz)] 2. *Inorganic chemistry* **2009**, *48* (23), 10865–10867.
(19) Chatterjee, S.; Norton, A. E.; Krause, J. A.; Oliver, A. G.; Abdolmaleki, M. K.; Barker, N. M.; Connick, W. B. Vapochromic and Vapoluminescent Sensors: Optical Versions of Electronic Noses. *Organic and Inorganic Materials Based Sensors* **2024**, *1*, 329–367.
(20) Norton, A. E.; Zanoni, K. P. S.; Dourges, M.-A.; Ravaro, L. P.; Abdolmaleki, M. K.; Camargo, A. S. S. de; Toupance, T.; Connick, W. B.; Chatterjee, S. Porosity Induced Rigidochromism in Platinum(II) Terpyridyl Luminophores Immobilized at Silica

Composites. *J. Mater. Chem. C* **2021**, *9* (19), 6193–6207. https://doi.org/10.1039/D1TC00599E.
(21) Norton, A. E.; Abdolmaleki, M. K.; Ringo, J. M.; Shingade, V. M.; Cashen, C.; Sharma, M.; Connick, W. B.; Chatterjee, S. A Colorimetric/Luminescence Sensor for Detecting MeCN in Water: Towards Direct Detection of Dissolved Organic Contaminants. *Sensors and Actuators B: Chemical* **2021**, *329*, 129207. https://doi.org/10.1016/j.snb.2020.129207.
(22) D. Taylor, S.; E. Norton, A.; T. Hart, R.; K. Abdolmaleki, M.; A. Krause, J.; B. Connick, W. Between Red and Yellow: Evidence of Intermediates in a Vapochromic Pt(Ii) Salt. *Chemical Communications* **2013**, *49* (80), 9161–9163. https://doi.org/10.1039/C3CC45418E.
(23) Norton, A. E.; Abdolmaleki, M. K.; Zhao, D.; Taylor, S. D.; Kennedy, S. R.; Ball, T. D.; Bovee, M. O.; Connick, W. B.; Chatterjee, S. Vapoluminescence Hysteresis in a Platinum (II) Salt-Based Humidity Sensor: Mapping the Vapochromic Response to Water Vapor. *Sensors and Actuators B: Chemical* **2022**, *359*, 131502.
(24) Abdolmaleki, M. K.; Riasi, M. S.; Enayati, M.; Norton, A. E.; Chatterjee, S.; Yeghiazarian, L.; Connick, W. B.; Abbaspourrad, A. A Digital Imaging Method for Evaluating the Kinetics of Vapochromic Response. *Talanta* **2020**, *209*, 120520.
(25) Guardado-Alvarez, T. M.; Chen, W.; Norton, A. E.; Russell, M. M.; Connick, W. B.; Zink, J. I. Analyte-Responsive Gated Hollow Mesoporous Silica Nanoparticles Exhibiting Inverse Functionality and an AND Logic Response. *Nanoscale* **2016**, *8* (43), 18296–18300.
(26) Norton, A. E.; Abdolmaleki, M. K.; Andriot, L.; Cashen, C.; Krause, J. A.; Connick, W. B.; Chatterjee, S. Optical Sensing of Aqueous Nitrate Anion by a Platinum (Ii) Triimine Salt Based Solid State Material. *Chemical Communications* **2022**, *58* (87), 12160–12163.
(27) Norton, A. E.; Sharma, M.; Cashen, C.; Dourges, M.-A.; Toupance, T.; Krause, J. A.; Motkuri, R. K.; Connick, W. B.; Chatterjee, S. pH-Mediated Colorimetric and Luminescent Sensing of Aqueous Nitrate Anions by a Platinum(II) Luminophore@Mesoporous Silica Composite. *ACS Appl. Mater. Interfaces* **2021**, *13* (14), 16197–16209. https://doi.org/10.1021/acsami.0c20821.
(28) D. Taylor, S.; Howard, W.; Kaval, N.; Hart, R.; A. Krause, J.; B. Connick, W. Solid-State Materials for Anion Sensing in Aqueous Solution: Highly Selective Colorimetric and Luminescence-Based Detection of Perchlorate Using a Platinum(Ii) Salt. *Chemical Communications* **2010**, *46* (7), 1070–1072. https://doi.org/10.1039/B923278H.
(29) Chatterjee, S.; Norton, A. E.; Edwards, M. K.; Peterson, J. M.; Taylor, S. D.; Bryan, S. A.; Andersen, A.; Govind, N.; Albrecht-Schmitt, T. E.; Connick, W. B. Highly Selective Colorimetric and Luminescence Response of a Square-Planar Platinum (II) Terpyridyl Complex to Aqueous TcO4–. *Inorganic Chemistry* **2015**, *54* (20), 9914–9923.
(30) Bryant, M.; Skelton, J.; Hatcher, L.; Stubbs, C.; Madrid, E.; Pallipurath, A. R.; Thomas, L.; Woodall, C.; Christensen, J.; Fuertes, S. A Rapidly-Reversible Absorptive and Emissive Vapochromic Pt (II) Pincer-Based Chemical Sensor. *Nature communications* **2017**, *8* (1), 1800.
(31) Wadas, T. J.; Wang, Q.-M.; Kim, Y.; Flaschenreim, C.; Blanton, T. N.; Eisenberg, R. Vapochromism and Its Structural Basis in a Luminescent Pt (II) Terpyridine− Nicotinamide Complex. *Journal of the American Chemical Society* **2004**, *126* (51), 16841–16849.
(32) Field, J. S.; Grimmer, C. D.; Munro, O. Q.; Waldron, B. P. Speciation in Solution, Solid State Spectroscopy and Vapochromism of [Pt (Trpy)(NCS)] SbF 6 Where Trpy= 2, 2′: 6′, 2″-Terpyridine. *Dalton Transactions* **2010**, *39* (6), 1558–1567.

(33) Kato, M.; Yoshida, M.; Sun, Y.; Kobayashi, A. New Aspects of Vapochromic Metal Complexes: Cooperative Phenomena in Functions and Structures. *Journal of Photochemistry and Photobiology C: Photochemistry Reviews* **2022**, *51*, 100477. https://doi.org/10.1016/j.jphotochemrev.2021.100477.
(34) Zhang, R.; Liang, Z.; Han, A.; Wu, H.; Du, P.; Lai, W.; Cao, R. Structural, Spectroscopic and Theoretical Studies of a Vapochromic Platinum (II) Terpyridyl Complex. *CrystEngComm* **2014**, *16* (25), 5531–5542.
(35) Miskowski, V. M.; Houlding, V. H. Electronic Spectra and Photophysics of Platinum(II) Complexes with .Alpha.-Diimine Ligands. Solid-State Effects. 1. Monomers and Ligand .Pi. Dimers. *Inorg. Chem.* **1989**, *28* (8), 1529–1533. https://doi.org/10.1021/ic00307a021.

Data is available upon request